

Article

Identifying Spatial Priority of Ecological Restoration Dependent on Landscape Quality Trends in Metropolitan Areas

Junda Huang¹, Yuncai Wang^{1,2,*}  and Lang Zhang³

¹ Department of Landscape Architecture, College of Architecture and Urban Planning, Tongji University, Shanghai 200092, China; 1810172@tongji.edu.cn

² Center of Ecological Planning and Environment Effects Research, Key Laboratory of Ecology and Energy-Saving Study of Dense Habitat, Ministry of Education, Shanghai 200092, China

³ Shanghai Academy of Landscape Architecture Science and Planning, Shanghai 200232, China; zl@shsyky.com

* Correspondence: wyc1967@tongji.edu.cn; Tel.: +86-021-65980253

Abstract: Ecological restoration has become an important tool for mitigating and adapting to environmental degradation caused by global urbanization. However, current research has focused on single indicators and qualitative analysis, meaning that ecological restoration has not been effectively and comprehensively addressed. This study constructed a spatial priority identification system for ecological restoration, with landscape area, landscape structure and landscape function as the core indicators. The system has wide adaptability. In this work, the spatial classification of ecological degradation was performed by overlay analysis. The results showed the following: (1) In the Shanghai metropolitan area, the landscape quality showed a trend of degradation, with built-up areas encroaching on forests and cropland. (2) Ecological degradation in the suburbs was more severe than that in the urban center. Forests had the highest landscape area indicator (LAI) stability. Significant degradation of landscape structure indicators (LSIs) occurred when built-up area and cropland were transformed into forests. (3) Different types of ecological restoration had significant spatial distribution patterns. Through this identification system, this study aimed to help planners/managers of ecological restoration to recognize the changing patterns of regional landscape quality and its relationship with land cover. It ultimately provides a basis for the formulation of regional ecological objectives and spatial strategies.

Keywords: ecological degradation; landscape area; landscape structure; landscape function; restoration classification; long time-series analysis; land cover evolution



Citation: Huang, J.; Wang, Y.; Zhang, L. Identifying Spatial Priority of Ecological Restoration Dependent on Landscape Quality Trends in Metropolitan Areas. *Land* **2022**, *11*, 27. <https://doi.org/10.3390/land11010027>

Received: 23 November 2021

Accepted: 22 December 2021

Published: 24 December 2021

Publisher's Note: MDPI stays neutral with regard to jurisdictional claims in published maps and institutional affiliations.



Copyright: © 2021 by the authors. Licensee MDPI, Basel, Switzerland. This article is an open access article distributed under the terms and conditions of the Creative Commons Attribution (CC BY) license (<https://creativecommons.org/licenses/by/4.0/>).

1. Introduction

In recent years, cities, as human settlements, have seen continuous expansion of their built-up areas in efforts to meet the growing needs of mankind [1]. From 2001 to 2018, the global built-up area increased from 7.47×10^5 km² to 8.0×10^5 km² [2]. With the population gathering, industrial upgrading, and the spread of rapid transportation, metropolitan areas are emerging globally as large, highly integrated regions [3]. However, humanity's growing ecological footprint has altered the original vegetation, climate systems, and material and energy cycles [4]. These changes have led to numerous urban risks, such as the urban heat island (UHI) effect, air pollution, and urban flooding, which severely limit the sustainable development of cities [5–7]. Therefore, in metropolitan areas, the study of landscape status, change processes, and ecological restoration has become a worldwide research hotspot [8].

Landscape quality as a term to measure spatial quality has an extensive definition that includes many factors, such as environmental pollution and cleanliness, visual and aesthetic quality, and regional ecological benefits [9]. Thus, the evaluation of landscape quality should include a broader analysis of the structure and relationships between the different landscape elements. In this study, landscape quality was defined and understood as the state in which the landscape area, structure, and function is found at a given time.

This quality is an effect superimposed on a set of environmental components, processes, and phenomena that is the direct result of human activity (e.g., urbanization and spatial design) or indirect influence (e.g., agriculture and industry) [10]. In other words, the change in urban landscape quality is more influenced by human disturbance than natural factors [11].

Under the influence of long-term human activities, the regional landscape quality will be degraded, and the resilience to external disturbances and ecological stability and other natural regulation functions will be reduced [12]. When spaces with high-level landscape quality are degraded to low-level ones, it is mainly reflected in the reduction in vegetation area and quantity and in the decrease in structural connectivity and stability [13,14]. Currently, the most common and generally accepted indicators are those related to landscape ecology, which also have the advantage of being applicable to any geographical environment [15].

On the one hand, many researchers have studied the objective evaluation of landscapes. Landscape pattern indicators are the most common evaluation metrics. Such indicators have been used by scholars to evaluate the variability of study areas from different scales, times, and regional perspectives. For instance, existing studies have proven keen to explore the spatial and temporal variability of landscape quality across different regions [16], to analyze the scale effects of individual landscape elements (green spaces and water bodies) [17], and to model the influence of land use on landscape quality [18]. In particular, landscape connectivity has been explored in many studies as an important part of evaluating landscape quality. Some studies have quantified landscape connectivity through spatial metrics, such as COHESION metrics or dispersal range [19,20]. Some scholars have applied morphological spatial pattern analysis (MSPA) to analyze the fragmentation of ecological networks and to monitor ecological changes in different periods [21].

On the other hand, research on ecological restoration focuses on the influential mechanisms of biotic and abiotic factors, which means analyzing the transitions of plant and animal communities, the quality of abiotic elements, and the differences between geographical environments during the degradation of landscape quality [22–24]. In addition, some studies have used landscape pattern indicators and statistical models to extract ecological information from large-scale areas in order to explore the characteristics and processes of landscape quality degradation. These data are used to restore ecological networks and to identify the priorities of ecosystem services [25–29].

With advancements in remote sensing technology and the accumulation of data, it has become possible to detect and evaluate regional landscape quality changes in the long term [30–32]. For instance, in the Guangdong–Hong Kong–Macau Greater Bay Area, Yang et al. integrated vegetative cover, the vegetation health index, the normalized differential build-up and bare soil index, land surface moisture, and land surface temperature to construct a comprehensive index to describe the spatial and temporal variation characteristics of landscape quality [33]. Figueira Branco et al. evaluated the temporal trends in vegetation patterns within the Sooretama Biological Reserve and its surroundings, located in the north of Espírito Santo state, Brazil, and found that the Vegetation Condition Index had a potential for drought occurrence analysis in regions and areas with different vegetation densities [34].

However, most studies have focused on the qualitative analysis of ecological status [35]. Some were biased toward individual indicators, and few conducted comprehensive evaluations from multiple dimensions [36,37]. Fewer researchers still have further analyzed the priority of regional ecological restoration. As a complex, dynamic ecosystem, the regional landscape cannot rely on a single feature to summarize its transformation; various factors, such as area, structure, and function, should also be taken into account [38]. A framework for intuitive and effective ecological restoration, in conjunction with the gradual development of the region, is required, especially in a global first-tier city with a high population density.

To fill the gaps in existing studies, this study proposed an integrated approach to evaluate ecological restoration priorities based on regional landscape quality tendencies, taking the Shanghai metropolitan area as the study site. The results should help urban planners/managers to recognize the objective rules of landscape quality in different regions. More importantly, spatial prioritization of landscape quality can be identified to point to regions that need optimal protection. Furthermore, targeted restoration measures can be implemented according to different types of degradation. The specific aims of this study were as follows: (1) to develop a comprehensive index system with wide applicability to quantitatively analyze the regional landscape area, landscape structure, and landscape function; (2) to reveal trends in landscape quality over a long time series and explore the relationship between land cover and landscape quality; and (3) to identify the most degraded areas of landscape quality and classify the types of ecological restoration under different degradation levels.

2. Study Site

The Shanghai metropolitan area is located on the west coast of the Pacific Ocean, the eastern edge of the Asian continent (120°52' to 122°12' E, 30°40' to 31°53' N). The total area of the region is 6340 km², and the landform type is mainly plain, part of the alluvial plain of the Yangtze River Delta. It has a subtropical humid monsoon climate with four distinct seasons, sufficient sunshine, and abundant rainfall. During July and August, the study site experiences abundant rainfall, as well as the densest vegetation foliage. The land cover type appears different, with the outer ring as the dividing line. The region within the outer ring is dominated by residential and commercial land, with a lack of natural vegetation cover [39]. The region beyond the outer ring, with large areas of secondary forest, has an inland lake (Taihu Lake) and numerous water nets (Figure 1).

As an important economic, transportation, technology, financial, and shipping center in China, Shanghai is one of the world's largest metropolitan areas [40]. Compared to other metropolitan areas in the world, the Shanghai metropolitan area, on the one hand, is located on an impact plain, which is similar to many metropolitan areas, such as Tokyo, New York, and Jakarta [41]. The flat terrain is conducive to promoting urbanization and industrial gathering, while the concentration of population and industrial development also mean that the regional ecology suffers more disturbances.

On the other hand, metropolitan areas share a similar demographic background. For example, Tokyo and New York have population densities of 14,386 and 28,490 inhabitants/km², respectively [42,43]. For the Shanghai metropolitan area, by the end of 2020, the population density was about 23,092 inhabitants/km², which is lower than the 24,137 inhabitants/km² in 2010 (Shanghai Statistics Bureau, 2020). This phenomenon implies a population flow to regions outside the urban center, which is also reflected in the development of the rest of the metropolitan area. High-density habitation inevitably leads to the spread of grey infrastructure, meaning that the Shanghai metropolitan area is facing landscape quality degradation and land-use conflicts [44].

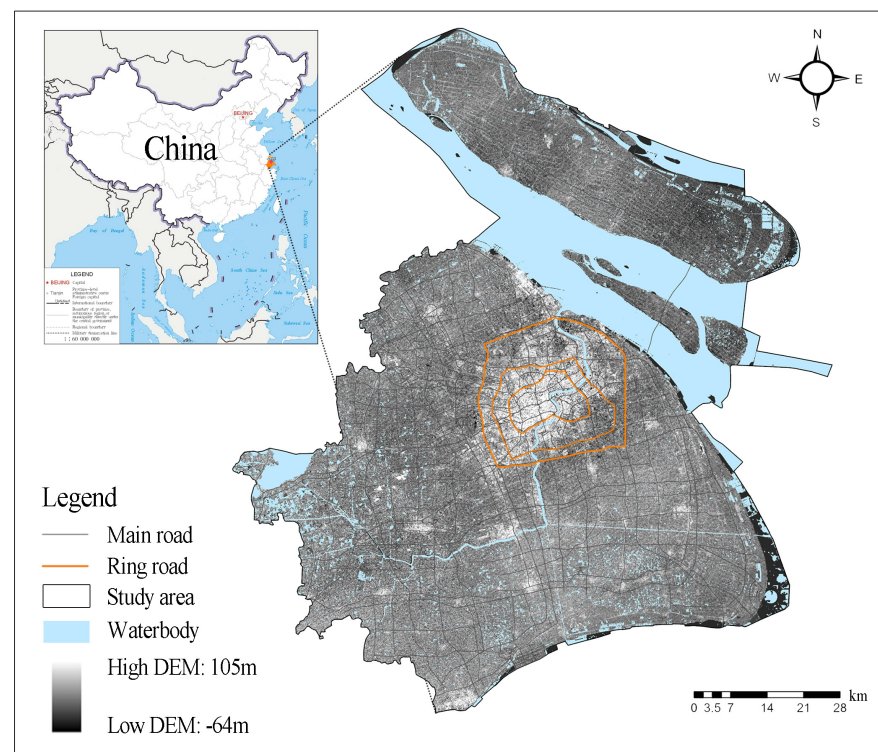


Figure 1. Study site: topography and urban space in 2020.

3. Materials and Methods

3.1. Data and Processing

Remote sensing images (RSIs), a digital elevation model (DEM), and Google HD imagery were used as the primary data to analyze landscape quality and land cover characteristics and changes in the study site. RSIs were downloaded from the USGS website (<https://glovis.usgs.gov/app>, accessed on 21 November 2021). DEM was collected from the Data Center for Resource and Environmental Sciences, Chinese Academy of Sciences (<http://www.resdc.cn/>, accessed on 21 November 2021), with a resolution of $30\text{ m} \times 30\text{ m}$.

Through field surveys and consultation with experts from the Shanghai Greening Bureau and Environmental Protection Bureau, it should be noted that around the year 2005, numerous policies were introduced in the Shanghai metropolitan area, resulting in large-scale landscape changes. The data used in this study are detailed in Table 1. For each year, two remote sensing images needed to be stitched together to extract the extent of the Shanghai metropolitan area (WRS_PATH = 118, WRS_ROW = 038 and WRS_PATH = 118, WRS_ROW = 039).

Data from all nine years were used to identify trends in landscape quality. The data of the starting year 2007 and the final year 2020 were used to classify the land cover. The land cover was classified into five categories based on the geography of Shanghai and the land classification in existing urban planning, which contains built-up area, water bodies, cropland, forest, grassland, and barren land. The Region of Interest (ROI) tool was used to create 100 samples for each category of land cover. We ensured that the separation value of ROI was greater than 1.9, which indicated that they were qualified samples. Finally, the maximum likelihood estimation was applied to supervise the classification of land cover in the study site [45]. In addition, the confusion matrix method was chosen for the accuracy validation of the classification results [46]. In total, 100 sample squares were selected separately for each land cover type using Google HD images and field surveys. The accuracy statements were obtained by selecting Confusion Matrix Using Ground Truth

ROIs in ENVI 5.3. The results showed that the classification accuracy was above 85%, which satisfied the requirements.

Table 1. Data information used in this study.

Name	Date	Source/Resolution (m)	Pro-Processing
DEM	—	ASTER GDEM/30 m	
HD imagery	Same year as remote sensing images	Google Earth Pro/1 m	
RSI	8 September 2005	Landsat 5/30 m	Data were pre-processed by Radiometric Calibration and FLAASH Atmospheric Correction tools in ENVI 5.3.
RSI	28 July 2007	Landsat 5/30 m	
RSI	19 September 2009	Landsat 5/30 m	
RSI	29 August 2013	Landsat 8/30 m	
RSI	3 August 2015	Landsat 8/30 m	
RSI	27 July 2016	Landsat 8/30 m	
RSI	24 August 2017	Landsat 8/30 m	
RSI	29 July 2019	Landsat 8/30 m	
RSI	16 August 2020	Landsat 8/30 m	

Meanwhile, the transition matrix was used to analyze the changes in land cover within the Shanghai metropolitan area, comparing the differences in land cover between 2007 and 2020 [47]. In this study, the proportion of land cover types in 2007 was set as Equation (1), and the proportion of land in category j in 2020 was set as Equation (2).

$$C_{i+} = \sum_{i=1}^n C_{ij}, \quad (1)$$

$$C_{+j} = \sum_{j=1}^n C_{ij}, \quad (2)$$

where C_{ij} ($i \neq j$) represents the proportion of land cover shifted from type i to type j between 2007 and 2020, and n is the total number of land cover types. The diagonal entries, C_{jj} , represent the proportion of land cover that shows the persistence of type j [48].

$Loss_i$ represents the reduction in land cover in type i , which is equal to the difference between C_{i+} and C_{ii} . $Loss_j$ represents the total increase in land cover in type j from 2007 to 2020, which is equal to the difference between C_{+j} and C_{jj} [49].

$$Loss_i = C_{i+} - C_{ii}, \quad (3)$$

$$Loss_j = C_{+j} - C_{jj}. \quad (4)$$

3.2. Landscape Quality Index System

With landscape ecology as the theoretical basis of research, this study considered the spatial and temporal changes in the landscape in the regional ecosystem. By analyzing existing studies, indicators characterizing three dimensions of landscape area, landscape structure, and landscape function were selected to construct an index system of landscape quality in the Shanghai metropolitan area.

1. Landscape area indicator (LAI)

There are differences in the ability of various landscape types to maintain ecosystem structure and function and to resist external disturbances [30]. This is directly affected by the area occupied by the land cover type. The landscape area is a visual representation of the change in the regional ecosystem and an important indicator of the landscape quality. The enhanced vegetation index (EVI) is similar to the normalized difference vegetation index (NDVI). However, EVI corrects for some atmospheric conditions and canopy background noise and is more sensitive in regions with dense vegetation, compensating for the inability of NDVI to correct for changes in solar incidence angle [50]. Therefore, this study chose

EVI to quantify the degree of variation in regional LAI change [51]. The equation for the LAI is as follows:

$$\text{LAI} = (\text{EA} - \text{IA}) / \text{IA} * 100\%, \quad (5)$$

where EA is the value of EVI in the late year (refers to the areas in years 2007, 2009, 2013, 2015, 2017, and 2020). IA is the value of EVI for the year earlier than EA (refers to the areas in years 2005, 2007, 2009, 2013, 2015, and 2017, corresponding to the year of EA).

2. Landscape structure indicator (LSI)

To quantify the shape and configuration of the regional landscape, the LSI was constructed by fusing the fractal dimension index (*FRAC*) and the contiguity index (*CONTAG*). It is important to note that for LSI, the target was all land cover types, excluding barren land and built-up area. On the one hand, *FRAC* is often used to quantitatively describe the size of the core area and the clutter of the boundaries of a patch [52]. Compared to other landscape metrics that describe spatial patterns, such as the shape index, the mean perimeter–area ratio (*PARA_MN*), and *MSPA*, *FRAC* compensates for some shortcomings through algorithms. First, it overcomes the main limitation of *PARA_MN* in measuring shape complexity [53]. Second, *FRAC* solves the dimensional dependence problem, which is caused by the calculation of the perimeter area ratio as a shape complexity metric [54]. Thus, *FRAC* was chosen to describe the shape of landscape patches. The calculation formula is as follows:

$$\text{FRAC} = \frac{2 \times \ln(0.25P_{ij})}{\ln A_{ij}}, \quad (6)$$

where P_{ij} = perimeter (m) of the patch ij , and A_{ij} = area (m^2) of the patch ij . The range of *FRAC* is 1 to 2. The closer the *FRAC* is to 2, the more fragmented the patch's shape is (i.e., the more it is disturbed by human activities). The units: none.

The contiguity index (*CONTAG*) was used to assess the spatial connectivity and continuity within the raster cells, which can reflect the degree of fragmentation and the interference of human activities [55]. For example, landscapes with a few large, continuous patches (containing most internal units with similar proximity) may have higher values of *CONTAG*. Thus, compared to the interspersion and juxtaposition index (based on patch adjacencies), *CONTAG* can visualize the dispersion and interspersion of landscape patches by their numerical size [52]. The calculation formula is as follows:

$$\text{CONTIG} = \frac{\left[\frac{\sum_{r=1}^z c_{ijr}}{a_{ij}} \right] - 1}{v - 1}, \quad (7)$$

where c_{ijr} = contiguity value for pixel r in patch ij , v = sum of the values in a 3-by-3 cell template, and a_{ij} = area of patch ij in terms of the number of cells. The range of *CONTIG* is 0–1. The closer the value of *CONTIG* is to 0, the more it represents an increase in the continuity or connectivity of the patch. In addition, it can also represent a decrease in patch connectivity. The units: none.

The LSI was composed of *FRAC* and *CONTAG* together. It should be noted that *FRAC* and *CONTIG* are both dimensionless indicators, but their values have different trends. When the value of *FRAC* and *CONTIG* is smaller, the shape of the patch is more regular, but the connectivity is worse. Thus, while normalizing the data, the value of *FRAC* needs to be inverted, which means that when the value of *FRAC* is smaller, the patch's shape is more fragmented. The first component, which is LSI, is then obtained by principal component analysis (*PCA*). The formula is as follows:

$$\text{LSI} = \text{PCA}[f(\text{FRAC}, \text{CONTIG})], \quad (8)$$

The range of LSI is 0–1. The closer the value of LSI is to 0, the worse the connectivity of the patch and the more fragmented the shape. Moreover, it represents an increase in the morphological regularity and connectivity of the patch. The units: none.

3. Landscape function index (LFI)

Many studies have argued that heat, greenness, moisture, and dryness are closely related to the ecological functions corresponding to the ecosystem [26]. Any perturbation or change in these ecological factors will eventually act on the whole ecosystem [56,57]. The traditional evaluation method only incorporates a single type of remote sensing data into the index system. However, some indicators are difficult to obtain directly by remote sensing, such as surface air temperature, which can often have significant bias by inversion only [58]. Using a combination of multiple layers of remote sensing as the input data set for LFI is a good way to reduce error and attenuate the effect of a single type of dataset.

Land surface temperature (LST), normalized difference vegetation index (NDVI), WET, and normalized differential build-up and bare soil index (NDBSI), corresponding to heat, greenness, moisture, and dryness, respectively, have been widely used to evaluate landscape quality [59]. Therefore, this study obtained four indicators by band calculation [60]. They were then normalized from 0 to 1. Finally, the first component was taken to represent LFI by PCA [61]. The formula is as follows:

$$LFI = PCA[f(NDVI, WET, NDBSI, LST)]. \quad (9)$$

3.3. Tendency of Landscape Quality and Its Relationship to Land Cover Conversion

Tests for detecting trends in time-series data can be divided into parametric and non-parametric methods [62]. Non-parametric methods require only that the data be independent and insensitive to measurement errors and outlier data and to have been applied to the detection of time-series data in fields such as hydrology, meteorology, and vegetation [11,63]. The Mann–Kendall (MK) test, a widely used non-parametric statistical test, has the advantage that it does not require the measured values to follow a normal distribution and is not affected by missing values and outliers [64,65]. Therefore, this study used Mann–Kendall and Sen’s slope estimation to identify and test the trend of landscape quality in the Shanghai metropolitan area.

The statistic S of the MK test is calculated as follows [66]:

$$S = \sum_{i=1}^{n-1} \sum_{j=i+1}^n \text{sgn}(x_j - x_i), \quad (10)$$

where n is the number of data points, and x_i and x_j are the data values in time series i and j ($j > i$), respectively. The detailed calculation of $\text{sgn}(x_j - x_i)$ and the variance within Equation (10) can be found in the research of Milan Gocic et al. [62].

It should be noted that 8 years in the 2007–2020 time-series data were selected in this study, which means that $n \geq 8$. Mann et al. explained that when $n \geq 8$, S is almost normally distributed with consequent mean and variance [67,68].

The standard normal test statistic Z is expressed as

$$Z = \begin{cases} \frac{S}{\sqrt{\text{VAR}(S)}} & \text{if } S > 0 \\ 0 & \text{if } S = 0 \\ \frac{S+1}{\sqrt{\text{VAR}(S)}} & \text{if } S < 0 \end{cases} \quad (11)$$

A positive (negative) value of Z indicates that the data tend to increase (decrease) with time. Testing trends were carried out at the specific α significance level. When $Z > Z_{1-\alpha/2}$, the null hypothesis is rejected, and a significant trend exists. Significance levels $\alpha = 0.01$ and $\alpha = 0.05$ were used in this study. The null hypothesis of no trend was rejected for $|Z| > 1.96$ at a 5% significance level.

Sen's slope estimator (known as the Theil–Sen median method) is a robust non-parametric statistical trend calculation method [69]. The calculation formula is as follows:

$$Q_i = \frac{x_j - x_k}{j - k} \text{ for } i = 1, 2, \dots, N, \quad (12)$$

$$Q_{med} = \begin{cases} Q_{(n+1)/2} & N \text{ is odd} \\ \frac{1}{2}(Q_{N/2} + Q_{(N+2)/2}) & N \text{ is even} \end{cases} \quad (13)$$

where x_j and x_k are observations for years j and k ($j > k$), respectively; N is the number of time periods, $N = n(n - 1)/2$; and Q_{med} is the median of Q_i , whose value indicates the steepness of the data trend [62]. We applied the reclassification toolsets -1 for degradation, 0 for stability, and 1 for improvement.

Based on the trend analysis, the Z values were classified into 2 categories (significant and insignificant), and the Sen's slope estimator results were classified into 3 categories (degradation, stable, and improvement) and multiplied by the raster calculator. The final trend was divided into 5 levels: significant degradation (-2), slight degradation (-1), stable (0), slight improvement (1), and significant improvement (2). Each of these 5 levels was assigned to each raster as a quantitative value of landscape quality. In other words, each type of land cover that changed had a corresponding trend level. Meanwhile, each raster had a corresponding land cover type in 2020 (transformed from the different land cover types in 2007). Furthermore, the spaces of different degradation levels and the land cover types to which they belong could establish a one-to-one relationship. Based on the land cover transfer matrix, the percentage of different degradation grading in the transformation type could be calculated.

All steps were calculated with the software R 4.1.0 and graphically represented in ArcGIS Pro 2.0. The specific steps and code data were referenced in the package "trend" [70]. The data package "raster" was used for pixel-by-pixel analysis [71]. Based on the above, the "terra" package was added to the original code to enable parallel computation and increase the computation speed [72]. Details of all packages and R scripts can be found on the related web page (<https://cran.r-project.org/>, accessed on 21 November 2021).

3.4. Ecological Restoration Priorities

The identification of ecological restoration priorities by combining all indicators is a difficult task. There may be different dimensions and ranges of values among indicators. Therefore, first, all metrics were selected and constructed in a dimensionless and standardized operation to ensure that their values all ranged from 0 to 1. According to the expert survey (Supplementary), the indicators of the three dimensions were assigned equal weights. The spatial distribution of ecological degradation was calculated by the spatial overlay. Second, it was further divided into five grades using the natural break method to reflect the priority level of ecological restoration, implying that the more severe the degradation of landscape quality, the higher the corresponding grading of ecological restoration.

Furthermore, the following steps were followed to achieve the purpose of targeted ecological restoration in regions with low landscape quality, with the identification of regions in need of ecological restoration and those whose values of landscape quality indicators (LAI, LSI, and LFI) of -2 and -1 were selected for multi-layer overlay. When an indicator or multiple indicators were -2 , it signified that it was the dominant type of landscape quality degradation. Thus, the types of degradation dominated by different indicators were able to be classified into 8 types: Type A: degradation led by LFI; Type B: degradation led by LAI; Type C: degradation led by LSI; Type D: degradation co-led by LAI and LSI; Type E: degradation co-led by LAI and LFI; Type F: degradation co-led by LSI and LFI; Type G: no indicator as degradation led; and Type H: degradation co-led by LSI, LAI and LFI.

4. Results

4.1. Changes in Land Cover

The land cover types in the Shanghai metropolitan area in 2007 and 2020 are shown in Figure 2. In 2007, a large proportion of forests were distributed in the periphery of the Shanghai metropolitan area. Small- and medium-sized ponds and wetlands formed a nested relationship with cropland and grassland. Affected by rapid urbanization, it was expected to see a significant outward expansion of the urban center by 2020. Compared with 2007, excluding built-up area (68.2% of the land area), the main land cover in 2020 was cropland and forest, at 20.9% and 9.8%, respectively. From the urban center to the suburbs, the vegetation coverage showed a gradual trend of decreasing, with the existing forest concentrated in large open green spaces and the Lin-Gang Special Area [73]. Meanwhile, former ponds and rivers were encroached upon by built-up area, mainly in the western and northern tracts.

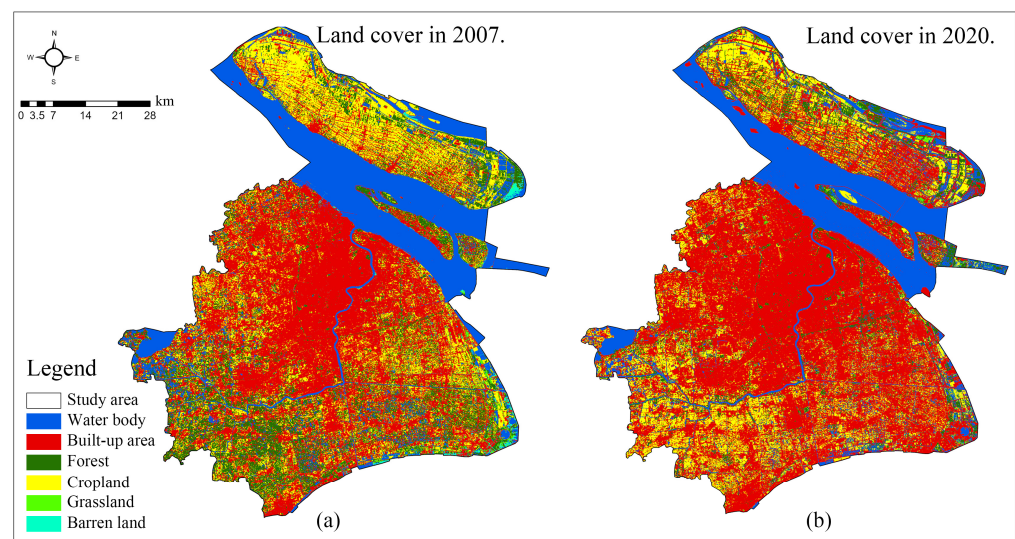


Figure 2. Distribution of different land cover types of the Shanghai metropolitan area in 2007 (a) and 2020 (b).

The total area of land cover transition during this period was about 3082.18 km². The land cover with the largest net increase in area was built-up area, mainly from the transition of cropland, forests, and water bodies. The land cover type with the first net reduction was cropland, which changed to forests and built-up area, at 14.14% and 46.30%, respectively (Table 2). Although 748.96 km² of cropland was turned into built-up area, the area of built-up area and forests that transformed into cropland was also sizeable (712.91 km²). The second largest reduction in land cover was water bodies, which mainly changed to built-up area, cropland, and forests, accounting for 53.16%, 25.40%, and 19.18% of the total converted area of water bodies, respectively. The grassland and barren land took up a smaller proportion of the area.

Table 2. Transition matrix of land cover from 2007 to 2020.

From 2007	To 2020						Area in 2007 (km ²)	Proportion ¹ (%)
	Water Bodies	Built-Up Area	Cropland	Forest	Grassland	Barren Land		
Water bodies	1257.42	187.89	89.78	67.79	5.33	2.67	1612.24	21.92
Built-up area	47.84	2967.92	245.10	108.93	9.50	5.83	3372.48	12.37
Cropland	68.96	748.96	542.34	228.75	20.24	8.09	1624.32	66.18

Table 2. Cont.

From 2007	To 2020						Area in 2007 (km ²)	Proportion ¹ (%)
	Water Bodies	Built-Up Area	Cropland	Forest	Grassland	Barren Land		
Forest	102.99	506.18	467.81	202.21	12.51	4.29	1295.39	84.44
Grassland	8.36	41.24	10.93	14.36	2.46	0.54	81.12	92.98
Barren land	13.77	37.65	5.99	8.50	1.40	0.58	70.91	94.92
Area in 2020 (km ²)	1499.34	4489.84	1361.95	630.54	51.44	22.00	—	—
Proportion ² (%)	83.87	66.10	39.82	32.07	4.78	2.64	—	—

Notes: The rows represent which types of land cover this category will be converted to from 2007 to 2020. The numbers on columns represent the area of this land cover type converted from other types in 2020. ¹ represents the percentage area of a land cover type converted to the remaining types compared to 2007. ² represents the percentage area of land cover type that has not been converted compared to the area of that type in 2020.

4.2. Grading of Landscape Quality Trends

As expected, the regions with low LAI in 2007 were concentrated in the port terminals and river banks. The regions with low LAI in 2020 gradually expanded to the periphery of the region and suburban villages. Meanwhile, the median of LAI in 2007 was larger than that in 2020 ($Med_{LAI,2007}$ is 0.707 and $Med_{LAI,2020}$ is 0.395), indicating that LAI decreased during this period and that the distribution of areas with lower LAI grew more concentrated. As a result of the multi-year trend analysis (Figure 3c1), there was 4684.23 km² of patches with LAI degradation from 2007 to 2020, or about 57.37% of the study site area. Significant degradation regions occupied 5.16%. However, in terms of total area, the difference between the improved and degraded areas of LAI was not significant. Regardless of whether in the urban center or the suburbs, the area (LAI improvement) was much larger than the degraded area. Meanwhile, compared to the suburbs, the proportion of patches, showing LAI improvement, was relatively higher in the urban center (Figure 3d1).

Figure 3a2,b2 show that the landscape structure of the Shanghai metropolitan area underwent degradation between 2007 and 2020. The LSI in 2007 was, on the whole, less disturbed by human activities. Only in Jinshan District and the Lin-Gang Special Area, where factories were concentrated, did the landscape structure show fragmentation. After 13 years of urbanization, the LSI of the study site declined in 2020, which was especially obvious in the coastal area. The area of degradation reached 1729.67 km², which is 68.2% of the total trend area. The rate of degradation was slower in the urban center compared to the suburbs (Figure 3d2). Moreover, the concentration of degraded LSI shifted from the southern part of Jinshan District to the periphery of this region (including Chongming Island), where the main land cover types were forests and cropland.

Comparing Figure 3a3,b3, the Shanghai metropolitan area also showed a significant degradation in LFI. Regions with low LFI in 2007 were restricted to the urban center and suburban villages, yet expanded to the entire metropolitan area by 2020. The number of regions exhibiting extremely low LFI increased. Only parts of the outer coastal areas, such as Chongming Island, showed green. In addition, we found that the trends in LFI were differentially distributed in the study site (Figure 3c3). On the one hand, regions with degradation covered more space (4560.44 km², 67.81%) compared to those with improved and stable LFI. On the other hand, the percentage of area with stable LFI in the urban center was 13.8%, larger than that in the suburbs. In the suburbs, there were more areas where LFI improved. The regions with a significant improvement in LFI were concentrated in the northern part of Chongming Island—mainly cropland and forests.

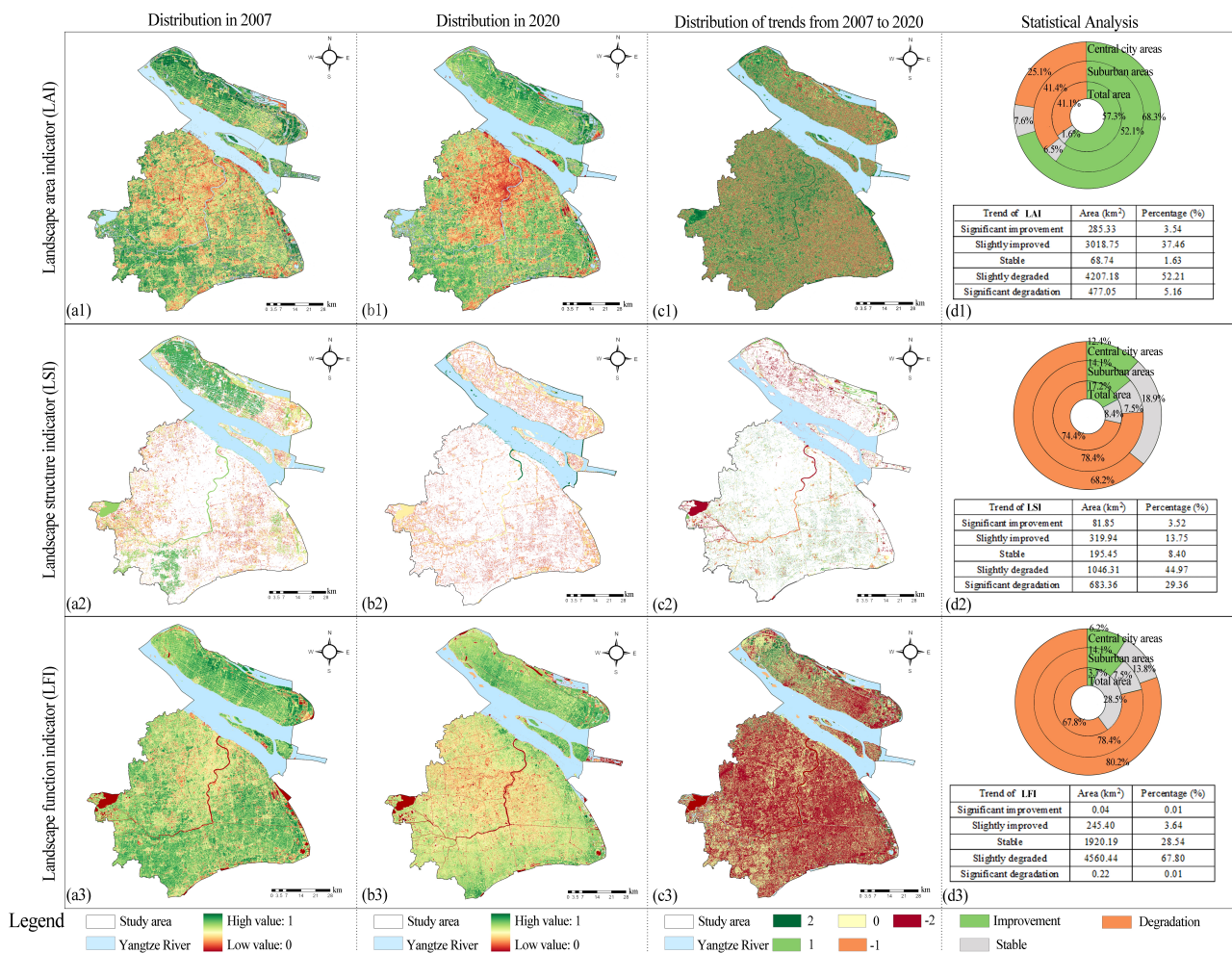


Figure 3. Distribution of landscape quality indicators in (a1–a3) 2007 and (b1–b3) in 2020, (c1–c3) trend distribution of landscape quality indicators from 2007 to 2020, and (d1–d3) the percentage of area classified by landscape quality indicator trends in different regions.

4.3. Relationship between Land Cover and Landscape Quality Indicators

Based on the change in land cover and trends of landscape quality from 2007 to 2020, compared to other land covers, the areas of water bodies, barren land, and grassland were rare, and their transition rates were low. Therefore, this study focused on the relationship between built-up area, forest, and cropland with landscape quality indicators. A two-by-two pairing of land cover and the type of its transfer was made through the grading of landscape indicators.

As can be seen from Table 3, the landscape quality of the same area changed to different degrees from 2007 to 2020. The landscape quality of land cover was mainly concentrated in the −1 to 1 grade range, which was similar to the trend in 2007 and 2020 for the same land cover type. Firstly, for LAI, the forests had the highest stability over long-term trends, whether from built-up area, cropland, or unconverted regions of the forest itself. However, water bodies had the second highest LAI variability, showing a stable or slightly degraded trend (degradation grades of 0 and −1 were in the range of 10–20%). Secondly, for LSI, the forests and water bodies showed a larger degree of degradation (the maximum percentage in −2 grade). It is noteworthy that the LSI of forests had an increasing trend on the +1 grade. Finally, for LFI, built-up area showed a significant trend of slight degradation (−1 grade, accounting for 20–70%). The process of mutual transition between forest and cropland also showed a slight degradation trend in the region.

Table 3. Relationship between land cover and landscape quality indicators from 2007 to 2020.

Land Cover in 2007	Land Cover in 2020	Area Percentage (%)					
		2 Level	1 Level	0 Level	−1 Level	−2 Level	
Built-up area (3372.48 km ²)	LAI	Water bodies	0.30	0.17	17.56	11.10	3.09
		Forest	0.40	0.30	47.71	0.91	0
		Cropland	0.50	0	1.84	0.20	0
		Grassland	0	0	0.3	0	0
	Built-up area	0	0	11.62	3.61	0.39	
	LSI	Water bodies	2.05	9.39	5.03	2.47	13.60
		Forest	1.15	14.77	4.78	7.48	18.63
		Cropland	0	0.51	0.21	0.32	0.78
		Grassland	0	0.25	0.58	0	0
	Built-up area	0.48	3.45	1.71	5.33	7.03	
	LFI	Water bodies	0.06	0.16	0.15	0.84	0.17
		Forest	0	0	0.46	2.31	0.41
		Cropland	0	0	0.92	5.22	1.03
		Grassland	0	0	0.3	0.21	0
	Built-up area	0	2.46	10.34	72.69	2.27	
	Forest (1295.39 km ²)	LAI	Water bodies	0	0.03	16.09	14.44
Forest			0	0.06	58.39	4.12	0
Cropland			0	0	1.61	0.06	0
Grassland			0	0	0.04	0	0
Built-up area		0	0	1.15	0.31	0.03	
LSI		Water bodies	1.41	11.37	4.71	3.86	13.06
		Forest	1.21	16.13	10.71	9.55	24.88
		Cropland	0	0.25	0.25	0.29	0.80
		Grassland	0	0	0	0	0.16
Built-up area		0	0.26	0.15	0.10	0.85	
LFI		Water bodies	0.28	1.49	2.27	3.40	0.46
		Forest	0	0.18	4.36	10.48	0.63
		Cropland	0	1.54	12.55	20.46	1.70
		Grassland	0	0	0.40	0.49	0
Built-up area		0	7.38	10.96	20.27	0.70	
Cropland (1624.32 km ²)		LAI	Water bodies	0	0	11.99	10.35
	Forest		0	0.03	66.95	5.38	0.03
	Cropland		0	0	2.12	0.08	0
	Grassland		0	0	0.07	0	0
	Built-up area	0	0	1.28	0.28	0	
	LSI	Water bodies	0.59	2.53	2.48	2.32	12.11
		Forest	0.54	11.55	8.16	5.77	50.31
		Cropland	0	0.15	0.12	0.13	1.70
		Grassland	0	0	0	0	0.06
	Built-up area	0	0.11	0.07	0.11	1.19	
	LFI	Water bodies	0.45	2.09	2.57	3.59	0.91
		Forest	0	1.03	8.32	10.83	1.84
		Cropland	0	1.37	7.70	16.50	3.87
		Grassland	0	0	1.52	0.86	0.10
	Built-up area	0.04	4.27	9.22	20.94	1.98	

Note: Color display rules for area percentage is 0 10 20 30 100.

When land cover areas with grades −2 and −1 were considered to have undergone degradation of landscape quality, the land cover transition patterns that showed the degradation were as follows (transition from the former type to the latter type): (1) for LAI, built-up area–water bodies, forest–water bodies, and cropland–water bodies; (2) for LSI, built-up area–forest, forest–forest, and cropland–forest; (3) for LFI, built-up area–built-up area, forest–cropland/built-up area, and cropland–cropland/built-up area.

4.4. Prioritization and Classification of Ecological Restoration

As shown in Figure 4a, the primary ecological restoration zone was 1160.62 km², the secondary ecological restoration zone was 3324.20 km², the ecological stable zone was 365.49 km², the weak ecological improvement zone was 1799.37 km², and the strong ecological improvement zone was 75.80 km². The priority restoration zone showed a pattern wherein the suburbs had more area than the urban center; see, for example, the external region of the outer ring, the northern part of Chongming Island, and the village agglomeration regions in the suburbs. The sub-restoration zone was widely distributed, spreading outward with the urban center as the core.

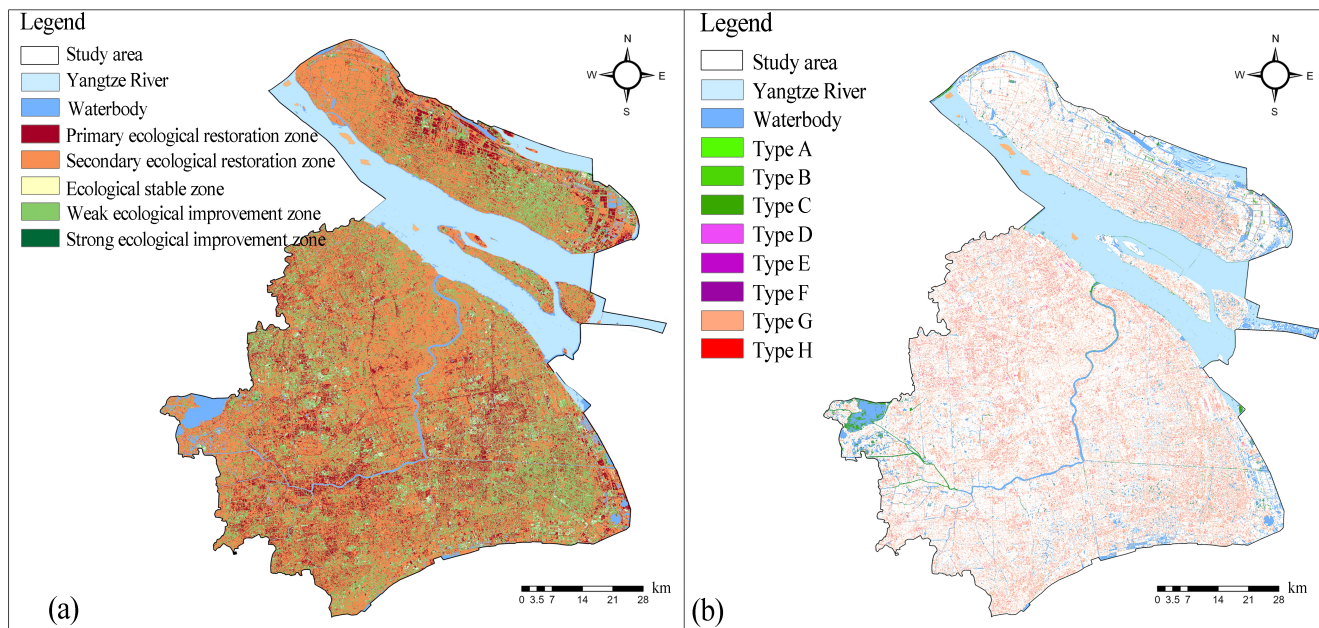


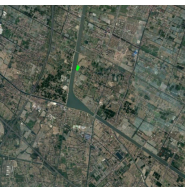
Figure 4. Spatial distribution of (a) ecological restoration priorities and (b) ecological restoration classification.

Furthermore, the regions with grades -2 and -1 were selected, in which the ecological restoration zones dominated by different landscape quality indicators could be visually identified. Figure 4b shows that Types B, C, D, and G have larger areas compared to the remaining types. Type B was primarily a green space near the port along the Puyang River, including residential and factory districts. Type C was distributed around linear roads and water bodies, with a discrete spatial distribution. Type D was mostly found near the built-up area and water bodies, dominated by public green space and woodland. Type G was the type with the largest area percentage and was distributed around cropland in the suburbs, showing a belt-shaped distribution and fragmented space (Table 4).

Table 4. Typical samples of ecological restoration based on different leading indicators.

Category	Dominant Indicator	Area (km ²)	Typical Sample	Category	Dominant Indicator	Area (km ²)	Typical Sample
Type A	The grading of LFI is -2 , when the grading of LAI and LSI is -1 .	0.522		Type E	The grading of LAI and LFI is -2 , when the grading of LSI is -1 .	0.048	

Table 4. Cont.

Category	Dominant Indicator	Area (km ²)	Typical Sample	Category	Dominant Indicator	Area (km ²)	Typical Sample
Type B	The grading of LAI is -2 , when the grading of LSI and LFI is -1 .	97.357		Type F	The grading of LSI and LFI is -2 , when the grading of LAI is -1 .	2.644	
Type C	The grading of LSI is -2 , when the grading of LAI and LFI is -1 .	502.990		Type G	The grading of LAI, LSI and LFI is -1 .	962.478	
Type D	The grading of LAI and LSI is -2 , when the grading of LFI is -1 .	97.403		Type H	The grading of LAI, LSI and LFI is -2 .	0.219	

5. Discussion

5.1. Trends of Landscape Quality in Metropolitan Areas

With the urbanization in the last decade, the difference in landscape quality between the urban center and the outer-ring regions is particularly significant. The urban center has high population densities and large impervious surfaces, which means fragmented green space, UHI effects, and dry surface environments [74,75]. This study found that the landscape quality of the Shanghai metropolitan area has shown a trend of degradation over long-term urbanization. Regions of low landscape quality in 2007 existed mainly in the urban center. In 2020, significant degradation and slight degradation spread across the boundaries of the urban center (the outer-ring road) and toward the distant suburbs. It is notable that the variation in low values of landscape quality indicators also showed a gradual shift from the urban center to the regional boundaries (Figure 3c1–c3), consistent with the stage of suburbanization development in the van den Berg model [76].

The reason for such a result is that, on the one hand, urban development is inevitably accompanied by the adaptation of the original environment. As the urban center is the core of the initial development, the land-use efficiency is usually high [77]. In spatially fixed areas, such as green infrastructure and built-up area, the trend of landscape quality is milder compared to that of the suburbs. On the contrary, the suburbs are vast and sparsely populated, where the inefficient use of land and waste of resources are common [78]. The land cover in the area studied was mostly secondary forest and cropland, which are sensitive to human activities (Figure 2). On the other hand, in China, the government-led land market is gradually improving, and the transformation of land properties depends on the implementation of urban planning. Notably, after the year 2000, the government gained control over the suburban districts and counties through administrative annexation [79], which led to the prevalence of land commoditization [80]. Suburbanization serves to satisfy the need to slow down capital flows and is driven by the potential devaluation of capital [81,82]. Consequently, suburbanization is occurring in many metropolitan areas around the world [83], leading to a gradual proliferation of human interventions in the environment [84]. These may explain the phenomena of the emergence of landscape quality in this study.

5.2. Drivers of Land Cover Transition on Landscape Quality

Landscape quality is inextricably linked to land cover type [85]. With the expansion of built-up area, the degradation of landscape quality spreads to the edge of metropolitan areas. From 2007 to 2020, built-up area encroached on about 1255 km² of forests and cropland. However, due to China's long-standing basic cropland protection policy and the strictly enforced green space target [86,87], a large amount of cropland and forests remain in the suburbs of the Shanghai metropolitan area (Figure 2).

This study found that the trend of LAI was stable, whether the land was built-up area, cropland converted to forests, or forests that remained unchanged, indicating that the transition of other types to forests did not lead to significant area loss in the Shanghai metropolitan area. This may explain the trend of a slightly improved LSI for the transition of built-up area and cropland to forests. However, the transition of built-up area–water bodies, forest–water bodies, and cropland–water bodies in LAI showed a degradation trend of regional LAI. On the one hand, this may require more area for water bodies in land transition compared to other land cover types, such as flood protection levees for rivers and the hardening of water bodies. On the other hand, remote sensing was taken in September, when the rainy season is over in Shanghai and the relative water level is low, which may also have led to degradation in the final results.

The results of LSI revealed that the percentage of significantly degraded area of cropland–forest was 55.31%. This means that the landscape structure can be severely affected by the process of reforestation. The ecological value of forests is higher than that of cropland, but in a region with a high degree of human activities, such as a metropolitan area, forests converted from cropland are the lands with lowest productivity [88]. These lands are limited in size and tend to form isolated islands of forest, which, in turn, reduce land connectivity [89]. However, 11.55% of the areas slightly improved during the transformation process, indicating that the possibility of LSI improvement still exists. This is consistent with the finding that a small amount of forest growth is beneficial for landscape connectivity, as found by Mrinmay Mandal et al. [90].

However, cropland is an important vehicle for maintaining regional biological flows and material exchange [91], which indicates that, when cropland is transformed into built-up area, it is often accompanied by a degradation of landscape quality. Therefore, maintaining the natural state of cropland and solving the problem of soil degradation/residue contamination can effectively guarantee the landscape function of the metropolitan area [92].

The results of the LFI showed significant degradation of built-up area–built-up area, forest–cropland/built-up area, and cropland–cropland/built-up area. The essential difference between forest, cropland, and built-up area is vegetation cover and impermeable surface [26]. Thus, the transition from forests and cropland to built-up area inevitably causes a reduction in LFI. It is noteworthy that a significant degradation of LFI also occurs when other land cover types are converted to cropland. Cropland (as a special type of land cover), different seasons, and crop varieties can lead to LFI changes [93–95]. Crops planted on cropland within the Shanghai metropolitan area were dominated by green leafy vegetables, rice, and fruit trees, implying that changes in crop species may have caused the degradation of LFI.

5.3. The Trade-Off between Ecological Restoration and Urban Development

This study found that the development of the Shanghai metropolitan area has mainly come at the expense of invading cropland and forests in the past decades. This is similar to the development pattern of many cities around the world [96]. However, the percentage of the priority restoration zone in the suburbs was much higher than in the urban center (Figure 4a), which can be attributed to a series of urban renewal and ecological restoration projects implemented by the government in the urban center [97]. The renewal and ecological restoration of central urban areas has been a hot research topic. The environmental integrity and sustainability of the built environments were improved through extensive land renewal and the replacement of functional regions [98]. Currently, the urban center is

dominated by secondary restoration areas and is mostly distributed in Type A, Type B, and Type D (Table 4). The main vegetation units in these regions include artificial grassland, water bodies, and riparian woodland. As new green spaces emerge, the quality of the new ecosystems does not fully match that of the original ecology [99], implying that ecological restoration needs to identify the original habitats.

Suburban villages, as regions where built-up area is gathered, were surrounded by secondary forests and cropland (Figure 3b1–b3). Green spaces of a certain area are preserved and planned within the villages, which may explain why Type G boasts the largest area and the most extensive coverage. As rivers and lakes are prone to fragmentation after being affected by human activities [100], Type C is distributed near natural water bodies (502.99 km²). Ecological restoration usually improves connectivity between fragmented patches by creating or restoring corridors and stepping stones [101]. Additionally, the implementation of ecological restoration also requires consideration of time costs due to the difference in the impact on landscape quality between the early and mid–late stages of urban development. Thus, depending on the stage, the capital investment for and implementation of ecological restoration must be adjusted [102], accelerating succession through integrated projects and restoring landscape quality to its pre-damaged state.

However, existing studies have caused controversy regarding the positive effects of ecological restoration projects on regional ecological quality. L-J Wang et al. found that the Grain for Green Program (GFGP) and the Natural Forests Conservation Program increased ecosystem values during 2000–2010 but decreased them during 2010–2015 [103]. Ecological restoration projects have a positive impact on the optimization of the structure of existing forests and the improvement in green cover [104,105]. The reasons for this could include, on the one hand, the climate and geography of the study site being highly differentiated, ensuring that the logic of ecological restoration can be applied in the face of geographically and climatically diverse regions. However, the results are prone to discrepancies [106]. On the other hand, the restoration of ecological quality has a time-lag effect [107]. The planning and implementation of ecological restoration projects are extremely complex from ecological, economic, and social perspectives [108]. In addition, there are many uncertainties in the evaluation of benefits after implementation [109].

5.4. Limitations and Future Research

In this study, the grading of ecologically degraded regions was achieved by analyzing trends in regional landscape quality and combining the transformation mechanism of land cover types. Additionally, eight types of ecological restoration requiring different strategies, were classified based on different factors that dominated the degradation. However, there were some limitations in this study.

First, Landsat series data with a resolution of 30m×30m were used in this study, and they have also been used in many other studies [110]. The differences in resolution of the research results need to be noted in subsequent studies. The remote sensing data used should be multi-sourced. For example, Sentinel-2 has higher accuracy multi-band remote sensing images, which are especially effective for monitoring vegetation health information [88]. Meanwhile, combining panchromatic bands with pan-sharpening of the original multispectral bands can effectively improve the resolution of the base data [111].

Second, this study comprehensively evaluated the trend changes in regional ecology through a multidimensional index system and identified regions with different levels of landscape quality. However, the essence of the study was still a characterization of regional ecology. Therefore, future research should explore the factors affecting ecological degradation retrospectively, such as economic factors and social development factors [112,113].

In addition, an analytical method based on geometric concepts, namely, the morphological spatial pattern analysis (MSPA), is widely used in the field of ecological sciences [16]. MSPA can visually reflect the spatial characteristics of regional ecology. In other words, the application of MSPA to analyze and identify trend changes in regional ecological spa-

tial structure could directly guide the adjustment and implementation of urban planning, which should be further explored in future research.

6. Conclusions

Ecological degradation has always been an issue of concern for economic and social development [114]. Taking the Shanghai metropolitan area as an example, this study provided a comprehensive evaluation of regional landscape quality through indicators in three dimensions: landscape area, structure, and function. These indicators covered the main characteristics of spatial changes in the landscape while remaining independent of the scale of the study unit. Trends in landscape quality over long periods of time were analyzed using Mann–Kendall and Sen’s slope estimator statistical tests. The results showed that, in the process of urban development, built-up areas in the Shanghai metropolitan area encroached on forests (506.18 km²) and cropland (748.96 km²) from 2007 to 2020. Furthermore, forests with stable LAI accounted for 47.71% of the whole study area and had the highest LAI stability compared to cropland and built-up area. When the built-up area and agricultural land were converted to forest, 18.63% and 50.31% of the land showed significant LSI degradation, respectively. The interconversion of forest and agricultural land affected about 10% of the land with LFI degradation, which meant that this behavior could lead to a slight degradation of landscape functions.

Based on the results of landscape quality, restoration priorities were identified, and different types of ecological restoration goals were set. We found that the suburbs warranted a much higher position of priority with respect to ecological restoration as compared to the urban center in terms of area and percentage. The most common types of ecological restoration in the Shanghai metropolitan area were Type C (covering 502.99 km²), where the degradation of the landscape structure was dominant, and Type G (covering 962.478 km²), with a slight degradation of landscape quality. This study highlights ecological restoration-oriented development planning in the Shanghai metropolitan area. The results illustrate the need to pay attention to the evolution process of landscape quality in long-term analysis under the premise of sustainable urban development. This can provide a more rapid scientific basis for ecological monitoring and urban planning.

Supplementary Materials: The following supporting information can be downloaded at: <https://www.mdpi.com/article/10.3390/land11010027/s1>, Expert Survey: A total of 23 professors and PhD students from universities around the world were consulted for this study. They are mainly from the School of Ecological and Environmental Sciences, East China Normal University; Sustainability Research Institute, School of Earth and Environment, University of Leeds; School of Architecture and Urban Planning, Tongji University; Henan Agricultural University, College of Landscape Architecture and Art.

Author Contributions: Conceptualization, J.H. and Y.W.; methodology, J.H.; software, J.H.; validation, J.H., Y.W., and L.Z.; formal analysis, J.H.; investigation, J.H.; resources, J.H.; data curation, L.Z.; writing—original draft preparation, J.H.; writing—review and editing, J.H.; visualization, J.H. and L.Z.; supervision, Y.W.; project administration, Y.W.; funding acquisition, Y.W. All authors have read and agreed to the published version of the manuscript.

Funding: This research was funded by the Shanghai Committee of Science and Technology Found “Research on Ecological Network Layout and System Optimization Technology” (No.19DZ1203303).

Acknowledgments: The authors are grateful to the anonymous reviewers and editors for their detailed comments and valuable suggestions.

Conflicts of Interest: The authors declare no conflict of interest.

References

1. Grimm, N.B.; Faeth, S.H.; Golubiewski, N.E.; Redman, C.L.; Wu, J.G.; Bai, X.M.; Briggs, J.M. Global change and the ecology of cities. *Science* **2008**, *319*, 756–760. [[CrossRef](#)] [[PubMed](#)]
2. Sun, L.; Chen, J.; Li, Q.; Huang, D. Dramatic uneven urbanization of large cities throughout the world in recent decades. *Nat. Commun.* **2020**, *11*, 5366. [[CrossRef](#)] [[PubMed](#)]

3. Squires, G. *Urban Sprawl: Causes, Consequences and Policy Responses*; Urban Institute Press: Washington, DC, USA, 2002.
4. Foley, J.A.; DeFries, R.; Asner, G.P.; Barford, C.; Bonan, G.; Carpenter, S.R.; Chapin, F.S.; Coe, M.T.; Daily, G.C.; Gibbs, H.K.; et al. Global consequences of land use. *Science* **2005**, *309*, 570–574. [[CrossRef](#)]
5. Yamashita, S.; Sekine, K. Some studies on the earth's surface conditions relating to the urban heat island. *Energy Build.* **1990**, *15*, 279–288. [[CrossRef](#)]
6. Khan, I.; Hou, F.; Le, H.P.; Ali, S.A. Do natural resources, urbanization, and value-adding manufacturing affect environmental quality? Evidence from the top ten manufacturing countries. *Resour. Policy* **2021**, *72*, 102109. [[CrossRef](#)]
7. Kc, S.; Shrestha, S.; Ninsawat, S.; Chonwattana, S. Predicting flood events in Kathmandu Metropolitan City under climate change and urbanisation. *J. Environ. Manag.* **2021**, *281*, 111894. [[CrossRef](#)]
8. Millennium Ecosystem Assessment. *Ecosystems and Human Well-Being: Biodiversity Synthesis*; World Resources Institute: Washington, DC, USA, 2005. Available online: <https://www.biodiversitylibrary.org/item/119291> (accessed on 21 November 2021).
9. Sargolini, M. Environmental and Landscape Quality. In *Urban Landscapes: Environmental Networks and Quality of Life*; Sargolini, M., Ed.; Springer: Milan, Italy, 2013; pp. 11–17. [[CrossRef](#)]
10. Vizzari, M. Spatial modelling of potential landscape quality. *Appl. Geogr.* **2011**, *31*, 108–118. [[CrossRef](#)]
11. Wang, W.J.; Wu, T.; Li, Y.Z.; Xie, S.L.; Han, B.L.; Zheng, H.; Ouyang, Z.Y. Urbanization Impacts on natural habitat and ecosystem services in the Guangdong-Hong Kong-Macao “Megacity”. *Sustainability* **2020**, *12*, 6675. [[CrossRef](#)]
12. Nilsson, C.; Grelsson, G. The Fragility of Ecosystems: A Review. *J. Appl. Ecol.* **1995**, *32*, 677–692. [[CrossRef](#)]
13. Nagendra, H.; Nagendran, S.; Paul, S.; Pareeth, S. Graying, greening and fragmentation in the rapidly expanding Indian city of Bangalore. *Landsc. Urban Plan.* **2012**, *105*, 400–406. [[CrossRef](#)]
14. Rebelo, A.G.; Holmes, P.M.; Dorse, C.; Wood, J. Impacts of urbanization in a biodiversity hotspot: Conservation challenges in Metropolitan Cape Town. *S. Afr. J. Bot.* **2011**, *77*, 20–35. [[CrossRef](#)]
15. Cassatella, C.; Voghera, A. Indicators Used for Landscape. In *Landscape Indicators: Assessing and Monitoring Landscape Quality*; Cassatella, C., Peano, A., Eds.; Springer: Dordrecht, The Netherlands, 2011; pp. 31–46. [[CrossRef](#)]
16. Luo, M.; Li, T. Spatial and temporal analysis of landscape ecological quality in Yulin. *Environ. Technol. Innov.* **2021**, *23*, 101700. [[CrossRef](#)]
17. Peng, S.; Li, S. Scale relationship between landscape pattern and water quality in different pollution source areas: A case study of the Fuxian Lake watershed, China. *Ecol. Indic.* **2021**, *121*, 107136. [[CrossRef](#)]
18. Darvishi, A.; Yousefi, M.; Marull, J. Modelling landscape ecological assessments of land use and cover change scenarios. Application to the Bojnourd Metropolitan Area (NE Iran). *Land Use Policy* **2020**, *99*, 105098. [[CrossRef](#)]
19. Wang, M.; Ma, Y.-f.; You, X.-y. An innovative approach to identify environmental variables with conservation priorities in habitat patches. *J. Environ. Manag.* **2021**, *292*, 112788. [[CrossRef](#)] [[PubMed](#)]
20. Zhang, Z.; Meerow, S.; Newell, J.P.; Lindquist, M. Enhancing landscape connectivity through multifunctional green infrastructure corridor modeling and design. *Urban For. Urban Green.* **2019**, *38*, 305–317. [[CrossRef](#)]
21. Modica, G.; Praticò, S.; Laudari, L.; Ledda, A.; Di Fazio, S.; De Montis, A. Implementation of multispecies ecological networks at the regional scale: Analysis and multi-temporal assessment. *J. Environ. Manag.* **2021**, *289*, 112494. [[CrossRef](#)]
22. Uroosa; Kazmi, S.S.U.H.; Rahman, M.S.; Xu, H. Use of biological trait analysis of periphytic protozoan assemblages for evaluating effects of harmful algal blooms on ecological quality status in marine ecosystem. *Mar. Pollut. Bull.* **2021**, *164*, 112083. [[CrossRef](#)]
23. López, E.; Patiño, R.; Vázquez-Sauceda, M.L.; Pérez-Castañeda, R.; Arellano-Méndez, L.U.; Ventura, R.; Heyer, L. Water quality and ecological risk assessment of intermittent stream-flow through mining and urban areas of San Marcos River sub-basin, Mexico. *Environ. Nanotechnol. Monit. Manag.* **2020**, *14*, 100369. [[CrossRef](#)]
24. Liang, D.; Wang, Q.; Wei, N.; Tang, C.; Sun, X.; Yang, Y. Biological indicators of ecological quality in typical urban river-lake ecosystems: The planktonic rotifer community and its response to environmental factors. *Ecol. Indic.* **2020**, *112*, 106127. [[CrossRef](#)]
25. Huang, L.; Wang, J.; Fang, Y.; Zhai, T.; Cheng, H. An integrated approach towards spatial identification of restored and conserved priority areas of ecological network for implementation planning in metropolitan region. *Sustain. Cities Soc.* **2021**, *69*, 102865. [[CrossRef](#)]
26. Boori, M.S.; Choudhary, K.; Paringer, R.; Kupriyanov, A. Eco-environmental quality assessment based on pressure-state-response framework by remote sensing and GIS. *Remote Sens. Appl. Soc. Environ.* **2021**, *23*, 100530. [[CrossRef](#)]
27. Wang, L.; Li, Z.; Wang, D.; Chen, J.; Liu, Y.; Nie, X.; Zhang, Y.; Ning, K.; Hu, X. Unbalanced social-ecological development within the Dongting Lake basin: Inspiration from evaluation of ecological restoration projects. *J. Clean. Prod.* **2021**, *315*, 128161. [[CrossRef](#)]
28. Shen, J.; Guo, X.; Wang, Y. Identifying and setting the natural spaces priority based on the multi-ecosystem services capacity index. *Ecol. Indic.* **2021**, *125*, 107473. [[CrossRef](#)]
29. Li, Y.-Y.; Zhang, Y.-Z.; Jiang, Z.-Y.; Guo, C.-X.; Zhao, M.-Y.; Yang, Z.-G.; Guo, M.-Y.; Wu, B.-Y.; Chen, Q.-L. Integrating morphological spatial pattern analysis and the minimal cumulative resistance model to optimize urban ecological networks: A case study in Shenzhen City, China. *Ecol. Process.* **2021**, *10*, 63. [[CrossRef](#)]
30. Ju, H.; Niu, C.; Zhang, S.; Jiang, W.; Zhang, Z.; Zhang, X.; Yang, Z.; Cui, Y. Spatiotemporal patterns and modifiable areal unit problems of the landscape ecological risk in coastal areas: A case study of the Shandong Peninsula, China. *J. Clean. Prod.* **2021**, *310*, 127522. [[CrossRef](#)]

31. Dindaroglu, T. Determination of ecological networks for vegetation connectivity using GIS & AHP technique in the Mediterranean degraded karst ecosystems. *J. Arid. Environ.* **2021**, *188*, 104385. [[CrossRef](#)]
32. Das, A.; Basu, T. Assessment of peri-urban wetland ecological degradation through importance-performance analysis (IPA): A study on Chatra Wetland, India. *Ecol. Indic.* **2020**, *114*, 106274. [[CrossRef](#)]
33. Yang, C.; Zhang, C.; Li, Q.; Liu, H.; Gao, W.; Shi, T.; Liu, X.; Wu, G. Rapid urbanization and policy variation greatly drive ecological quality evolution in Guangdong-Hong Kong-Macau Greater Bay Area of China: A remote sensing perspective. *Ecol. Indic.* **2020**, *115*, 106373. [[CrossRef](#)]
34. Figueira Branco, E.R.; Rosa dos Santos, A.; Macedo Pezzopane, J.E.; Banhos dos Santos, A.; Alexandre, R.S.; Bernardes, V.P.; da Silva, R.G.; de Souza, K.B.; Moura, M.M. Space-time analysis of vegetation trends and drought occurrence in domain area of tropical forest. *J. Environ. Manag.* **2019**, *246*, 384–396. [[CrossRef](#)]
35. Firozjaei, M.K.; Kiavarz, M.; Homae, M.; Arsanjani, J.J.; Alavipanah, S.K. A novel method to quantify urban surface ecological poorness zone: A case study of several European cities. *Sci. Total. Environ.* **2021**, *757*, 143755. [[CrossRef](#)] [[PubMed](#)]
36. Faisal, A.-A.; Kafy, A.-A.; Al Rakib, A.; Akter, K.S.; Jahir, D.M.A.; Sikdar, M.S.; Ashrafi, T.J.; Mallik, S.; Rahman, M.M. Assessing and predicting land use/land cover, land surface temperature and urban thermal field variance index using Landsat imagery for Dhaka Metropolitan area. *Environ. Chall.* **2021**, *4*, 100192. [[CrossRef](#)]
37. Cortelezzi, A.; Barranquero, R.S.; Marinelli, C.B.; Fernández San Juan, M.R.; Cepeda, R.E. Environmental diagnosis of an urban basin from a social-ecological perspective. *Sci. Total. Environ.* **2019**, *678*, 267–277. [[CrossRef](#)] [[PubMed](#)]
38. Wang, Y.; Huang, J.; Chen, C.; Shen, J.; Sheng, S. The cooling intensity dependent on landscape complexity of green infrastructure in the metropolitan area. *J. Environ. Eng. Landsc. Manag.* **2021**, *29*, 318–336. [[CrossRef](#)]
39. Yue, W.; Chen, Y.; Zhang, Q.; Liu, Y. Spatial Explicit Assessment of Urban Vitality Using Multi-Source Data: A Case of Shanghai, China. *Sustainability* **2019**, *11*, 638. [[CrossRef](#)]
40. Meligrana, J.; Ren, W.; Zhang, Z.; Anderson, B. Planning a mega-city's future: An evaluation of Shanghai's municipal land-use plan. *Town Plan. Rev.* **2008**, *79*, 267–293. [[CrossRef](#)]
41. Bean, W.T.; Sanderson, E.W. Using a spatially explicit ecological model to test scenarios of fire use by Native Americans: An example from the Harlem Plains, New York, NY, USA. *Ecol. Model.* **2008**, *211*, 301–308. [[CrossRef](#)]
42. Department of City Planning. Projected Population 2010–2040 Summary. Available online: <https://data.cityofnewyork.us/City-Government/Projected-Population-2010-2040-Summary/ph5g-sr3v> (accessed on 21 November 2021).
43. Tokyo Population 2021. Available online: <https://worldpopulationreview.com/world-cities/tokyo-population> (accessed on 21 November 2021).
44. Feng, R.; Wang, F.; Wang, K.; Xu, S. Quantifying influences of anthropogenic-natural factors on ecological land evolution in mega-urban agglomeration: A case study of Guangdong-Hong Kong-Macao greater Bay area. *J. Clean. Prod.* **2021**, *283*, 125304. [[CrossRef](#)]
45. Bhatta, B. Analysis of urban growth pattern using remote sensing and GIS: A case study of Kolkata, India. *Int. J. Remote. Sens.* **2009**, *30*, 4733–4746. [[CrossRef](#)]
46. Usman, M.; Liedl, R.; Shahid, M.A.; Abbas, A. Land use/land cover classification and its change detection using multi-temporal MODIS NDVI data. *J. Geogr. Sci.* **2015**, *25*, 1479–1506. [[CrossRef](#)]
47. Pontius, R.G.; Shusas, E.; McEachern, M. Detecting important categorical land changes while accounting for persistence. *Agric. Ecosyst. Environ.* **2004**, *101*, 251–268. [[CrossRef](#)]
48. Lü, D.; Gao, G.; Lü, Y.; Xiao, F.; Fu, B. Detailed land use transition quantification matters for smart land management in drylands: An in-depth analysis in Northwest China. *Land Use Policy* **2020**, *90*, 104356. [[CrossRef](#)]
49. Braimoh, A.K. Random and systematic land-cover transitions in northern Ghana. *Agric. Ecosyst. Environ.* **2006**, *113*, 254–263. [[CrossRef](#)]
50. Landsat Missions. Landsat Enhanced Vegetation Index. Available online: <https://www.usgs.gov/landsat-missions/landsat-enhanced-vegetation-index> (accessed on 21 November 2021).
51. Gobron, N.; Pinty, B.; Verstraete, M.; Widlowski, J.L. Advanced vegetation indices optimized for up-coming sensors: Design, performance, and applications. *IEEE Trans. Geosci. Remote Sens.* **2000**, *38*, 2489–2505. [[CrossRef](#)]
52. McGarigal, K.S.; Marks, B.J. *FRAGSTATS: Spatial Pattern Analysis Program for Categorical Maps*; Department of Agriculture, Forest Service, Pacific Northwest Research Station: Corvallis, OR, USA, 1995; p. 122. [[CrossRef](#)]
53. Jia, Y.; Tang, L.; Xu, M.; Yang, X. Landscape pattern indices for evaluating urban spatial morphology—A case study of Chinese cities. *Ecol. Indic.* **2019**, *99*, 27–37. [[CrossRef](#)]
54. Alphan, H. Multi-temporal analysis of urbanisation patterns as coastal development indicators: Eastern Mediterranean coast of Turkey. *Ecol. Indic.* **2021**, *121*, 106994. [[CrossRef](#)]
55. Cengiz, S.; Görmüş, S.; Oğuz, D. Analysis of the urban growth pattern through spatial metrics; Ankara City. *Land Use Policy* **2021**, *112*, 105812. [[CrossRef](#)]
56. Leemhuis, C.; Thonfeld, F.; Näschen, K.; Steinbach, S.; Muro, J.; Strauch, A.; López, A.; Daconto, G.; Games, I.; Diekkrüger, B. Sustainability in the food-water-ecosystem nexus: The role of land use and land cover change for water resources and ecosystems in the Kilombero Wetland, Tanzania. *Sustainability* **2017**, *9*, 1513. [[CrossRef](#)]
57. Titova, J.; Baltrėnaitė, E. Physical and chemical properties of biochar produced from sewage sludge compost and plants biomass, fertilized with that compost, important for soil improvement. *Waste Biomass Valorization* **2021**, *12*, 3781–3800. [[CrossRef](#)]

58. Vancutsem, C.; Ceccato, P.; Dinku, T.; Connor, S.J. Evaluation of MODIS land surface temperature data to estimate air temperature in different ecosystems over Africa. *Remote Sens. Environ.* **2010**, *114*, 449–465. [CrossRef]
59. Xu, H.; Wang, Y.; Guan, H.; Shi, T.; Hu, X. Detecting ecological changes with a Remote Sensing Based Ecological Index (RSEI) produced time series and change vector analysis. *Remote Sens.* **2019**, *11*, 2345. [CrossRef]
60. Boori, M.S.; Choudhary, K.; Paringer, R.; Kupriyanov, A. Spatiotemporal ecological vulnerability analysis with statistical correlation based on satellite remote sensing in Samara, Russia. *J. Environ. Manag.* **2021**, *285*, 112138. [CrossRef] [PubMed]
61. Abson, D.J.; Dougill, A.J.; Stringer, L. Using Principal Component Analysis for information-rich socio-ecological vulnerability mapping in Southern Africa. *Appl. Geogr.* **2012**, *35*, 515–524. [CrossRef]
62. Gocic, M.; Trajkovic, S. Analysis of changes in meteorological variables using Mann-Kendall and Sen's slope estimator statistical tests in Serbia. *Glob. Planet. Chang.* **2013**, *100*, 172–182. [CrossRef]
63. da Silva, R.M.; Santos, C.A.G.; Moreira, M.; Corte-Real, J.; Silva, V.C.L.; Medeiros, I.C. Rainfall and river flow trends using Mann-Kendall and Sen's slope estimator statistical tests in the Cobres River basin. *Nat. Hazards* **2015**, *77*, 1205–1221. [CrossRef]
64. Forthofer, R.N.; Lehnen, R.G. Rank Correlation Methods. In *Public Program Analysis: A New Categorical Data Approach*; Forthofer, R.N., Lehnen, R.G., Eds.; Springer: Boston, MA, USA, 1981; pp. 146–163. [CrossRef]
65. Hamed, K.H. Trend detection in hydrologic data: The Mann-Kendall trend test under the scaling hypothesis. *J. Hydrol.* **2008**, *349*, 350–363. [CrossRef]
66. Warren, J. Statistical methods for environmental pollution monitoring. *Technometrics* **1988**, *30*, 348. [CrossRef]
67. Das, S.; Sangode, S.J.; Kandekar, A. Recent decline in streamflow and sediment discharge in the Godavari basin, India (1965–2015). *Catena* **2021**, *206*, 105537. [CrossRef]
68. Mann, H.B. Nonparametric tests against trend. *Econometrica* **1945**, *13*, 245–259. [CrossRef]
69. Sen, P.K. Estimates of the regression coefficient based on Kendall's Tau. *J. Am. Stat. Assoc.* **1968**, *63*, 1379–1389. [CrossRef]
70. Pohlert, T. Trend: Non-Parametric Trend Tests and Change-Point Detection. Available online: <https://cran.r-project.org/web/packages/trend/index.html> (accessed on 21 November 2021).
71. Hijmans, R.J.; van Etten, J.; Sumner, M.; Cheng, J.; Baston, D.; Bevan, A.; Bivand, R.; Busetto, L.; Canty, M.; Fasoli, B.; et al. Raster: Geographic Data Analysis and Modeling. Available online: <https://cran.r-project.org/web/packages/raster/index.html> (accessed on 21 November 2021).
72. Hijmans, R.J.; Bivand, R.; Forner, K.; Ooms, J.; Pebesma, E. Terra: Spatial Data Analysis. Available online: <https://cran.r-project.org/web/packages/terra/index.html> (accessed on 21 November 2021).
73. Pudong Shanghai. Lin-gang Special Area. 2021. Available online: http://english.pudong.gov.cn/2021-04/14/c_88754.htm (accessed on 21 November 2021).
74. Alberti, M. The effects of urban patterns on ecosystem function. *Int. Reg. Sci. Rev.* **2005**, *28*, 168–192. [CrossRef]
75. Silva, J.S.; da Silva, R.M.; Santos, C.A.G. Spatiotemporal impact of land use/land cover changes on urban heat islands: A case study of Paço do Lumiar, Brazil. *Built. Environ.* **2018**, *136*, 279–292. [CrossRef]
76. Kabisch, N.; Haase, D. Diversifying European agglomerations: Evidence of urban population trends for the 21st century. *Popul. Space Place* **2011**, *17*, 236–253. [CrossRef]
77. Van Grunsven, L. Compact cities: Sustainable urban forms for developing countries. *J. Hous. Built Environ.* **2003**, *18*, 387–391. [CrossRef]
78. Zhang, Z.; Liu, J.; Gu, X. Reduction of industrial land beyond Urban Development Boundary in Shanghai: Differences in policy responses and impact on towns and villages. *Land Use Policy* **2019**, *82*, 620–630. [CrossRef]
79. Zhang, J.; Wu, F. China's changing economic governance: Administrative annexation and the reorganization of local governments in the Yangtze River Delta. *Reg. Stud.* **2006**, *40*, 3–21. [CrossRef]
80. Xu, J.; Yeh, A. Decoding urban land governance: State reconstruction in contemporary Chinese cities. *Urban Stud.* **2009**, *46*, 559–581. [CrossRef]
81. Cox, K.R. The problem of metropolitan governance and the politics of scale. *Reg. Stud.* **2010**, *44*, 215–227. [CrossRef]
82. Shen, J.; Wu, F. The suburb as a space of capital accumulation: The development of new towns in Shanghai, China. *Antipode* **2017**, *49*, 761–780. [CrossRef]
83. Kovács, Z.; Harangozó, G.; Szigeti, C.; Koppány, K.; Kondor, A.C.; Szabó, B. Measuring the impacts of suburbanization with ecological footprint calculations. *Cities* **2020**, *101*, 102715. [CrossRef]
84. Mieszkowski, P.; Mills, E.S. The causes of metropolitan suburbanization. *J. Econ. Perspect.* **1993**, *7*, 135–147. [CrossRef]
85. Turner, B.L.; Kates, R.W.; Meyer, W.B. The earth as transformed by human action in retrospect. *Ann. Assoc. Am. Geogr.* **1994**, *84*, 711–715. [CrossRef]
86. Wu, Y.; Shan, L.; Guo, Z.; Peng, Y. Cultivated land protection policies in China facing 2030: Dynamic balance system versus basic farmland zoning. *Habitat Int.* **2017**, *69*, 126–138. [CrossRef]
87. Wu, W.-B.; Ma, J.; Meadows, M.E.; Banzhaf, E.; Huang, T.-Y.; Liu, Y.-F.; Zhao, B. Spatio-temporal changes in urban green space in 107 Chinese cities (1990–2019): The role of economic drivers and policy. *Int. J. Appl. Earth Obs. Geoinf.* **2021**, *103*, 102525. [CrossRef]
88. Trac, C.J.; Schmidt, A.H.; Harrell, S.; Hinckley, T.M. Is the returning farmland to forest program a success? Three case studies from Sichuan. *Environ. Pract.* **2013**, *15*, 350–366. [CrossRef] [PubMed]

89. Olejniczak, M.J.; Spiering, D.J.; Potts, D.L.; Warren, R.J., II. Urban forests form isolated archipelagos. *J. Urban Ecol.* **2018**, *4*, juy007. [[CrossRef](#)]
90. Mandal, M.; Das Chatterjee, N. Forest landscape and its ecological quality: A stepwise spatiotemporal evaluation through patch-matrix model in Jhargram District, West Bengal State, India. *Reg. Sustain.* **2021**, *2*, 164–176. [[CrossRef](#)]
91. Andrén, O.; Lindberg, T.; Paustian, K.; Rosswall, T. Ecology of arable land—Organisms, carbon and nitrogen cycling. *Biol. Conserv.* **2001**, *56*, 243–244. [[CrossRef](#)]
92. Kanianska, R. Agriculture and Its Impact on Land-Use, Environment, and Ecosystem Services. In *Landscape Ecology. The Influences of Land Use and Anthropogenic Impacts of Landscape Creation*; Almusaed, A., Ed.; InTech: Rijeka, Croatia, 2016. Available online: <https://www.intechopen.com/chapters/51201> (accessed on 21 November 2021).
93. Xiong, Z. Simulated effects of cropland expansion on seasonal temperatures over China. *Phys. Chem. Earth Parts A/B/C* **2015**, *87–88*, 108–118. [[CrossRef](#)]
94. Yifru, B.A.; Chung, I.-M.; Kim, M.-G.; Chang, S.W. Assessing the effect of land/use land cover and climate change on water yield and groundwater recharge in East African Rift Valley using integrated model. *J. Hydrol. Reg. Stud.* **2021**, *37*, 100926. [[CrossRef](#)]
95. Zhou, D.; Xiao, J.; Frolking, S.; Liu, S.; Zhang, L.; Cui, Y.; Zhou, G. Croplands intensify regional and global warming according to satellite observations. *Remote Sens. Environ.* **2021**, *264*, 112585. [[CrossRef](#)]
96. Gounaridis, D.; Newell, J.P.; Goodspeed, R. The impact of urban sprawl on forest landscapes in Southeast Michigan, 1985–2015. *Landsc. Ecol.* **2020**, *35*, 1975–1993. [[CrossRef](#)]
97. Yang, Y.-R.; Chang, C.-h. An Urban Regeneration Regime in China: A case study of urban redevelopment in Shanghai’s Taipingqiao area. *Urban Stud.* **2007**, *44*, 1809–1826. [[CrossRef](#)]
98. Oyeboode, O. Insight into Urban Renewal as a Strategic Remedy for the Built Environment in Nigeria. *Eur. J. Adv. Eng. Technol.* **2018**, *5*, 665–676.
99. Almassi, B. Value disputes in urban ecological restoration: Lessons from the Chicago Wilderness. *Stud. Hist. Philos. Sci. Part A* **2021**, *87*, 93–100. [[CrossRef](#)]
100. Fuller, M.R.; Doyle, M.W.; Strayer, D.L. Causes and consequences of habitat fragmentation in river networks. *Ann. N. Y. Acad. Sci.* **2015**, *1355*, 31–51. [[CrossRef](#)] [[PubMed](#)]
101. Young, T. Restoration ecology: The new frontier, 2nd edition. *Restor. Ecol.* **2013**, *21*, 526. [[CrossRef](#)]
102. Adjei Mensah, C. Destruction of Urban Green Spaces: A Problem beyond Urbanization in Kumasi City (Ghana). *Am. J. Environ. Prot.* **2014**, *3*, 1–9. [[CrossRef](#)]
103. Wang, L.-J.; Ma, S.; Zhao, Y.-G.; Zhang, J.-C. Ecological restoration projects did not increase the value of all ecosystem services in Northeast China. *For. Ecol. Manag.* **2021**, *495*, 119340. [[CrossRef](#)]
104. Li, L.; Gou, M.; Wang, N.; La, L.; Liu, C. Do ecological restoration programs reduce forest fragmentation? Case study of the Three Gorges Reservoir Area, China. *Ecol. Eng.* **2021**, *172*, 106410. [[CrossRef](#)]
105. Zhou, Y.; Fu, D.; Lu, C.; Xu, X.; Tang, Q. Positive effects of ecological restoration policies on the vegetation dynamics in a typical ecologically vulnerable area of China. *Ecol. Eng.* **2021**, *159*, 106087. [[CrossRef](#)]
106. Klaus, V.H.; Kiehl, K. A conceptual framework for urban ecological restoration and rehabilitation. *Basic Appl. Ecol.* **2021**, *52*, 82–94. [[CrossRef](#)]
107. Hobbs, R.J.; Arico, S.; Aronson, J.; Baron, J.S.; Bridgewater, P.; Cramer, V.A.; Epstein, P.R.; Ewel, J.J.; Klink, C.A.; Lugo, A.E.; et al. Novel ecosystems: Theoretical and management aspects of the new ecological world order. *Glob. Ecol. Biogeogr.* **2006**, *15*, 1–7. [[CrossRef](#)]
108. Bullock, J.M.; Aronson, J.; Newton, A.C.; Pywell, R.F.; Rey-Benayas, J.M. Restoration of ecosystem services and biodiversity: Conflicts and opportunities. *Trends Ecol. Evol.* **2011**, *26*, 541–549. [[CrossRef](#)] [[PubMed](#)]
109. Holl, K.D.; Howarth, R.B. Paying for Restoration. *Restor. Ecol.* **2000**, *8*, 260–267. [[CrossRef](#)]
110. Koley, S.; Chockalingam, J. Sentinel 1 and Sentinel 2 for cropland mapping with special emphasis on the usability of textural and vegetation indices. *Adv. Space Res.* **2021**, *19*, 1140. [[CrossRef](#)]
111. Wu, L.; Yin, Y.; Jiang, X.; Cheng, T.C.E. Pan-sharpening based on multi-objective decision for multi-band remote sensing images. *Pattern Recognit.* **2021**, *118*, 108022. [[CrossRef](#)]
112. Sun, Q.; Zhang, P.; Jiang, W.; Qu, W.; Sun, Y.; Sun, D. Navigating local environment and scientific knowledge in dryland social-ecological systems through linking ecological policy-household interactions with land surface dynamics. *Land Use Policy* **2022**, *112*, 105863. [[CrossRef](#)]
113. Haskell, L.; Bonnedahl, K.J.; Stål, H.I. Social innovation related to ecological crises: A systematic literature review and a research agenda for strong sustainability. *J. Clean. Prod.* **2021**, *325*, 129316. [[CrossRef](#)]
114. Shrinkhal, R. Economics, Technology, and Environmental Protection: A Critical Analysis of Phytomanagement. In *Phytomanagement of Polluted Sites*; Pandey, V.C., Bauddh, K., Eds.; Elsevier: Amsterdam, The Netherlands, 2019; Chapter 22; pp. 569–580.